Current Optics and Photonics
Vol. 3, No. 3, June 2019, pp. 220-226

ISSN: 2508-7266(Print) / ISSN: 2508-7274(Online)
DOI: https://doi.org/10.3807/COPP.2019.3.3.220

# Simple Denoising Method for Novel Speckle-shifting Ghost Imaging with Connected-region Labeling

**Sheng Yuan*, Xuemei Liu, and Pibin Bing**

*Department of Information and Engineering, North China University of Water Resources and Electric Power, Zhengzhou 450046, China*

(Received August 15, 2018 : revised November 26, 2018 : accepted April 16, 2019)

A novel speckle-shifting ghost imaging (SSGI) technique is proposed in this paper. This method can effectively extract the edge of an unknown object without achieving its clear ghost image beforehand. However, owing to the imaging mechanism of SSGI, the imaging result generally contains serious noise. To solve the problem, we further propose a simple and effective method to remove noise from the speckle-shifting ghost image with a connected-region labeling (CRL) algorithm. In this method, two ghost images of an object are first generated according to SSGI. A threshold and the CRL are then used to remove noise from the imaging results in turn. This method can retrieve a high-quality image of an object with fewer measurements. Numerical simulations are carried out to verify the feasibility and effectiveness.

*Keywords* : Ghost imaging, Edge detection, Connected-region labeling
*OCIS codes* : (110.2970) Image detection systems; (110.1758) Computational imaging; (110.4280) Noise in imaging systems; (100.3020) Image reconstruction-restoration

## I. INTRODUCTION

Ghost imaging (GI), as a novel optical imaging technique, has been developed over the past two decades [1-7]. Different from classical optical imaging, GI requires two light beams: One is called the *reference arm*, which is recorded by a detector with spatial-resolution ability such as a charge-coupled device (CCD), while the other is the *object arm*, which is detected by a single-pixel detector (bucket detector) after the light interacts with the object to be measured. The object can be computationally imaged by correlating the detected data in the two arms. In 2008, Shapiro proposed a computational GI (CGI) technique that replaces the reference beam in the classical GI system with a virtual computational part [8]. Subsequently in 2009, Bromberg *et al.* designed an experimental system to verify the feasibility of CGI, in which a spatial light modulator (SLM) is used to generate a series of random intensity patterns as illuminations [9]. Owing to the imaging mechanism of CGI, the retrieved image generally contains serious noise, which has become an obstacle in some practical applications, although many efforts such as compressive GI [10], differential GI [11], normalized GI [12], and iterative GI [13, 14] have been made to improve the signal-to-noise ratio (SNR).

Edge detection based on CGI has currently become a hot research topic. In 2015, Liu *et al.* first proposed an edge-detection method based on gradient GI (GGI) [15]. This method can extract the edge in a direction according to the gradient angle adopted in the random patterns in CGI. Based on GGI, Mao *et al.* recently proposed the speckle-shift GI (SSGI) to extract the edge without prior knowledge of an object [16]. These methods can bring great convenience in object recognition, but the noise is still difficult to remove, and will further affect the accuracy of recognition. To improve the quality of edge detection, Wang and Ren *et al.* have successively proposed subpixel-speckle-shifting ghost imaging [17] and difference Fourier single-pixel imaging [18], which can fully remove random noise from the imaging results, but the number of measure-

*Corresponding author: shn.yuan@sohu.com, ORCID 0000-0002-7495-7070
Color versions of one or more of the figures in this paper are available online.

ments should be double or even triple the resolution of the detected image.

In this paper, we propose a novel SSGI method that can effectively extract the edge of an unknown object. In this method, the illumination intensity patterns can be structured in a computer beforehand, and only two groups of intensity patterns are used to project the object. Compared tto the existing SSGI method, the imaging speed and quality will be improved. However owing to the imaging mechanism of GI, the imaging result generally contains serious noise. To solve this problem, a simple and effective denoising method for SSGI with a connected-region labeling (CRL) algorithm is further explored. First, two edge images of an unknown object are extracted according to SSGI. A threshold and the CRL algorithm are then used to remove noise from the imaging results in turn. This method can realize the image of an object with high quality, using fewer measurements. The organization of this paper is as follows. In Section II, the principle of the novel SSGI with the Sobel operator is introduced. In Section III, the steps of the denoising method with CRL are described specifically. Numerical simulation results are presented in Section IV, and finally we conclude this paper in Section V.

## II. A NOVEL SSGI WITH THE SOBEL OPERATOR

In Ref. [16], the edge-detection methods using SSGI with the Laplacian operator, Standard operator, and Sobel operator have been demonstrated theoretically and experimentally. The results show that SSGI with the Sobel operator is robust in noisy environments. However, the intensity patterns used to illuminate the object are divided into 8 groups. Only one eighth of the intensity patterns are used to detect the edge in a corresponding direction, so the clarity of the imaging result will be poor if the number of measurements is insufficient. Here we introduce a novel SSGI technique with the Sobel operator, in which the intensity patterns are divided into two groups, *i.e.*

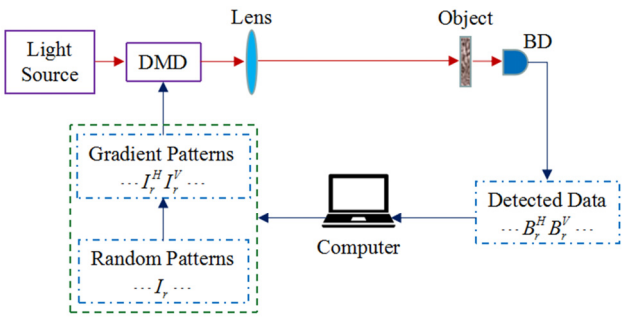


FIG. 1. Schematic diagram of the edge-detection system based on SSGI.

$$I_r^H(x,y) = I_r(x+1,y-1)+2I_r(x+1,y)+I_r(x+1,y+1) - I_r(x-1,y-1)-2I_r(x-1,y)-I_r(x-1,y+1) \quad (1)$$

and

$$I_r^V(x,y) = I_r(x-1,y+1)+2I_r(x,y+1)+I_r(x+1,y+1) - I_r(x-1,y-1)-2I_r(x,y-1)-I_r(x+1,y-1) \quad (2)$$

where $I_r^H(x,y)$ and $I_r^V(x,y)$ are the horizontal and vertical gradient patterns computed from an arbitrarily selected random intensity pattern $I_r(x,y)$, $r=1,2,\cdots M$, and $M$ is the number of measurements in the SSGI. All of these intensity patterns are computed and stored in the computer beforehand.

The setup for SSGI is schematically shown in Fig. 1. In the system, the series of structured patterns is generated by the computer-controlled digital micromirror device (DMD) and projected onto the object $O(x,y)$. The modulated light is finally collected by a single-pixel (bucket) detector (BD) to form the measurement data, *i.e.* $\{B_r^H\}$ and $\{B_r^V\}$,

$$B_r^H = \iint I_r^H(x,y)\,O(x,y)\,dxdy \quad (3)$$

and

$$B_r^V = \iint I_r^V(x,y)\,O(x,y)\,dxdy \quad (4)$$

The horizontal and vertical edge of the object are imaged by correlating the detected data with the random intensity patterns, *i.e.*,

$$E_H(x,y) = \frac{1}{M}\sum_{r=1}^{M}\left(B_r^H - \langle B^H\rangle\right)I_r(x,y) = \langle B^H I\rangle - \langle B^H\rangle\langle I\rangle \quad (5)$$

and

$$E_V(x,y) = \frac{1}{M}\sum_{r=1}^{M}\left(B_r^V - \langle B^V\rangle\right)I_r(x,y) = \langle B^V I\rangle - \langle B^V\rangle\langle I\rangle \quad (6)$$

where $\langle \bullet \rangle$ denotes the mean of the elements. The edge of the object is obtained by

$$E(x,y) = \sqrt{\left[E_H(x,y)\right]^2 + \left[E_V(x,y)\right]^2} \quad (7)$$

Further explanation of the edge-imaging process is presented in the appendix.

Compared to conventional SSGI [16], this method has two advantages. One is that the imaging speed will be increased, because the horizontal and vertical intensity patterns can be computed beforehand, and only two groups intensity patterns are used to illuminate the object; in conventional SSGI, eight groups of intensity patterns need to be generated by the DMD and projected onto the object. The other advantage is that the imaging result

may be clearer than that from SSGI with the same number of measurements. For example, 20,000 measurements are adopted in conventional SSGI, but only 2500 intensity patterns are used to extract the edge in one direction. In our method, the edge in the horizontal or vertical direction will be imaged by 10,000 measurements. Here, a binary image with 128 × 128 pixels (Fig. 2(a)) is adopted to verify the method's performance by numerical simulations. For comparison, the edge extracted from the original image by Sobel operator is shown in Fig. 2(b). One of the intensity patterns in the horizontal and vertical directions computed from Eqs. (1) and (2) is presented in Figs. 2(c) and 2(d) respectively. The horizontal and vertical edges of the object are imaged and shown in Figs. 2(e) and 2(f) respectively. Combining the two edge images according to Eq. (7), the result is shown in Fig. 2(g). As can be seen from the results, the edge imaged with our method is clearer than that from the conventional SSGI (Fig. 2(h)).

## III. DENOISING METHOD

Owing to the imaging mechanism of the speckle-pattern illumination, no matter for our method or the conventional SSGI, the detected results (Figs. 2(g) and 2(h)) generally contain serious noise, which may be an obstacle in some potential applications. Considering that the speckle noise is randomly distributed in the SSGI result, but the detected edge of the object is nearly fixed and constant, we therfore intend to reduce noise by comparing two SSGI results $E_1(x,y)$ and $E_2(x,y)$. The flow chart for the denoising method is shown in Fig. 3. According to the edge-detection results, an appropriate threshold is first set as

$$T=\mu+\sigma \tag{8}$$

where $\mu$ and $\sigma$ respectively denote the mean and standard deviation of $E(x,y)$. If $E_1(x,y)\geq T_1$ and $E_2(x,y)\geq T_2$, the position $(x,y)$ is believed to be the detected edge; otherwise, it is speckle noise. The preprocessing result can be mathematically expressed as

$$E_{th}(x,y)=\begin{cases}E_{sum}(x,y), & \text{if } E_1(x,y)\geq T_1 \text{ and } E_2(x,y)\geq T_2\\ 0, & \text{Otherwise}\end{cases} \tag{9}$$

where $E_{sum}(x,y)$ is the sum of the two SSGI results $E_1(x,y)$ and $E_2(x,y)$. Then the CRL, as a famous morphology algorithm [19, 20], is also used here to further reduce the small-speckle noise. We define the small-speckle area as $s<\epsilon s_{\max}$. The noise-reduction result using CRL can be written as

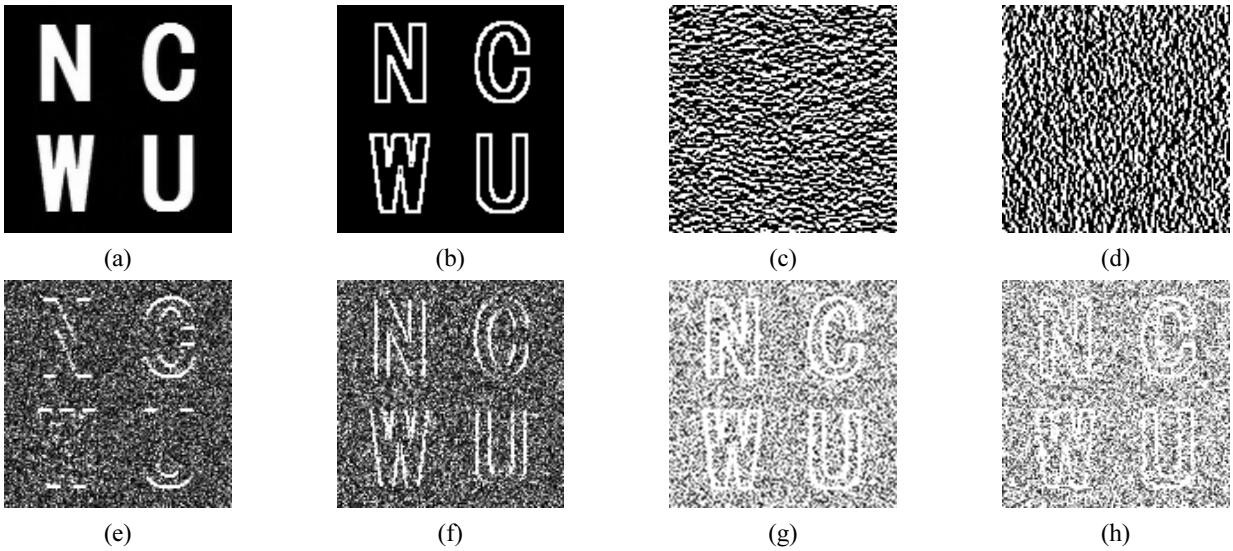


FIG. 2. Numerical simulation results for the novel and conventional SSGI techniques: (a) original image, (b) edge directly extracted from the object with the Sobel operator, (c) and (d) the horizontal and vertical intensity patterns, (e) and (f) the extracted horizontal and vertical edges, (g) and (h) the imaging results for the novel and conventional SSGI respectively.

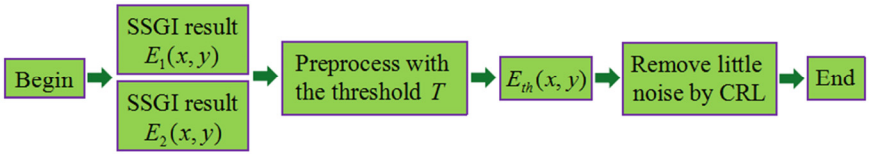


FIG. 3. Flow chart for the denoising method.

$$E_{CRL}(x,y)=\begin{cases}0, & \text{if } s<\epsilon s_{\max}\\ E_{th}(x,y) & otherwise\end{cases} \tag{10}$$

where $s_{\max}$ is the largest connected region and $\epsilon$ is a coefficient. In this method, the sparse matrix and Dulmage-Mendelsohn decomposition algorithm are used to label the largest connected region [21].

## IV. NUMERICAL SIMULATIONS

In this section, we will verify the feasibility of our proposed method by numerical simulations. To evaluate the quality of the detected edge, in this paper the peak signal-to-noise ratio (PSNR) is used as a metric, and defined as

$$\mathrm{PSNR}=-10*\lg\left\{\frac{\sum_{m=1}^{M}\sum_{n=1}^{N}[g'(x,y)-g(x,y)]^2}{(2^{k-1})^2 M\times N}\right\} \tag{11}$$

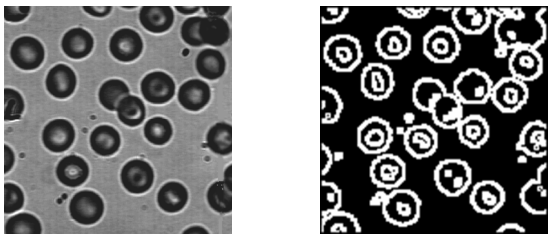

(a) (b)

FIG. 4. (a) The other object image, and (b) its edge, directly extracted with the Sobel operator.

where $g'(x,y)$ and $g(x,y)$ denote the detected result and reference image respectively. $M\times N$ is the size of the image, and $(2^k-1)$ represents the maximum grayscale value.

Apart from the binary image shown in Fig. 2(a), the grayscale image with 128 × 128 pixels shown in Fig. 4(a) is also adopted as the original object image in this simulation. The edge shown in Fig. 4(b) is directly extracted with the Sobel operator for comparison.

In the following simulations, 20,000 structured patterns are divided into two groups (*i.e.* 10,000 patterns in each group) to illuminate the object image, and each group will be used to generate a ghost image. Correlating the detected data with the structured patterns, the two edge images are generated by Eqs. (5)~(7) (*i.e.* the novel SSGI with the Sobel operator), and shown in Figs. 5(a), 5(b), 5(f) and 5(g) with PSNR = -2.18, -2.21, -6.11, and -6.09 dB respectively. As can be seen from the results, the edge looms through the speckle noise for both the binary and grayscale images. Because the noise is randomly distributed in the edge-detection results with the same probability, it will be tend to uniform in a superposition of the two results, which can be seen in Figs. 5(c) and 5(h). Subsequently using the threshold, the preprocessing results are obtained by Eq. (9) and shown in Figs. 5(d) and 5(i), respectively. Although most of the noise has been removed, some scattered noise still remains in the results. To further remove the small-speckle noise, the CRL algorithm is used here according to Eq. (10) for $\epsilon = 0.01$, and the results are shown in Figs. 5(e) and 5(j) with PSNR = 19.54 and 8.48 dB, corresponding to the binary and grayscale image respectively.

Apart from binary and grayscale images, the method proposed in this paper is also suitable for color images, because a color image can be decomposed into red (R), green (G), and blue (B) components. The connected region

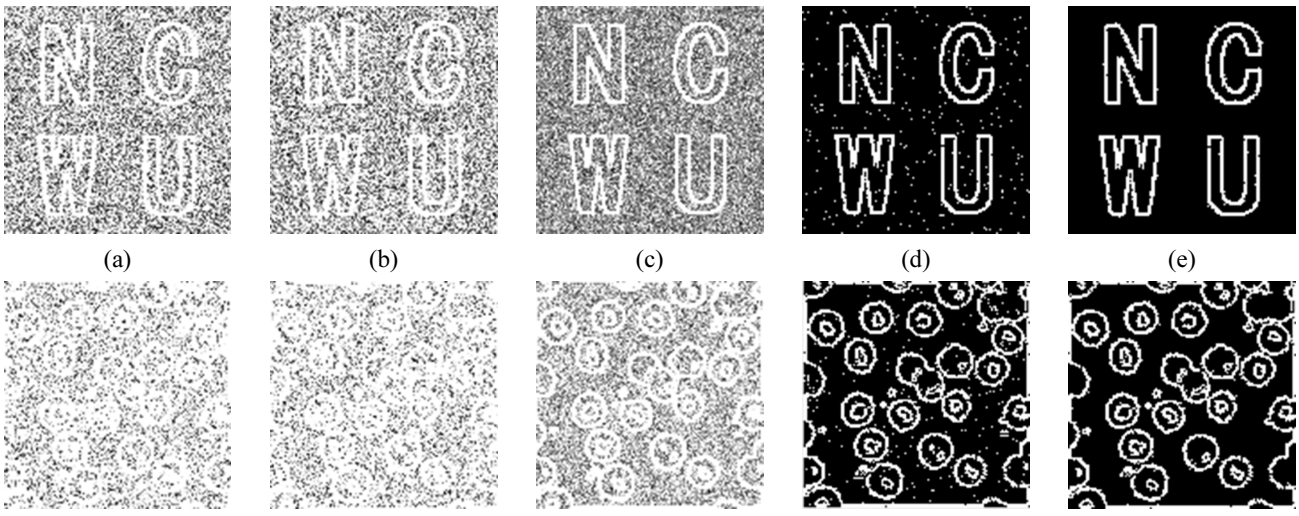

(a) (b) (c) (d) (e)

(f) (g) (h) (i) (j)

FIG. 5. Numerical simulation results for our proposed method in this paper, for number of measurements $M = 20000$ and coefficient $\epsilon = 0.01$ in CRL.

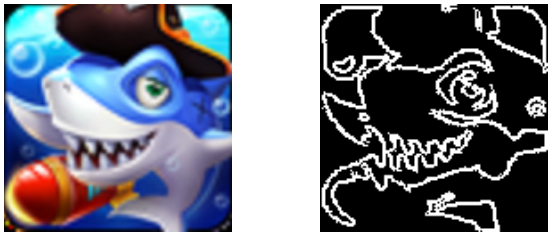

(a) (b)

FIG. 6. Simulation result for a color image: (a) original image, (b) edge extracted with the proposed method.

is labeled in a binary image, so the image retrieved with SSGI should be binarized at first, and the final extracted edge is binary. Figures 6(a) and 6(b) respectively present a color image and its extracted edge with this proposed method. We can see that the result is similar to that for the grayscale image.

Recently, Wang *et al.* have proposed an edge-detection method based on subpixel-shifting ghost imaging (SPSGI) [17]. According to the orthogonality of the Walsh-Hadamard matrix, the edge of an unknown object can be obtained with high quality and resolution by correlating the detected data with the subpixel-shifted Walsh-Hadamard patterns. In addition, Ren *et al.* have also proposed another edge-detection method with difference Fourier single-pixel imaging (DFSI) [18]. These two methods can extract the edge of an object with high quality, but the number of measurements should be at least double the resolution of the detected image for SPSGI, and triple for DFSI. Here we also take Figs. 2(a) and 4(a) as examples to numerically simulate the SPSGI and DFSI techniques.

When 32,768 Walsh-Hadamard patterns and 49,152 sinusoidal patterns are respectively used in SPSGI and DFSI, the edge is extracted clearly for both binary and grayscale images, as seen in Figs. 7(a)~7(d). However, when the number of measurements is insufficient, the imaging results blur. To intuitively observe the differences among the imaging results of these methods, 30,000 structured patterns are adopted to detect the edge of the binary image, and the results are shown on the right side of Fig. 8. As can be seen, the result is overlapped for SPSGI

(a) (b) (c) (d)

FIG. 7. Numerical simulation results for ((a) and (b)) SPSGI and ((c) and (d)) DFSI.

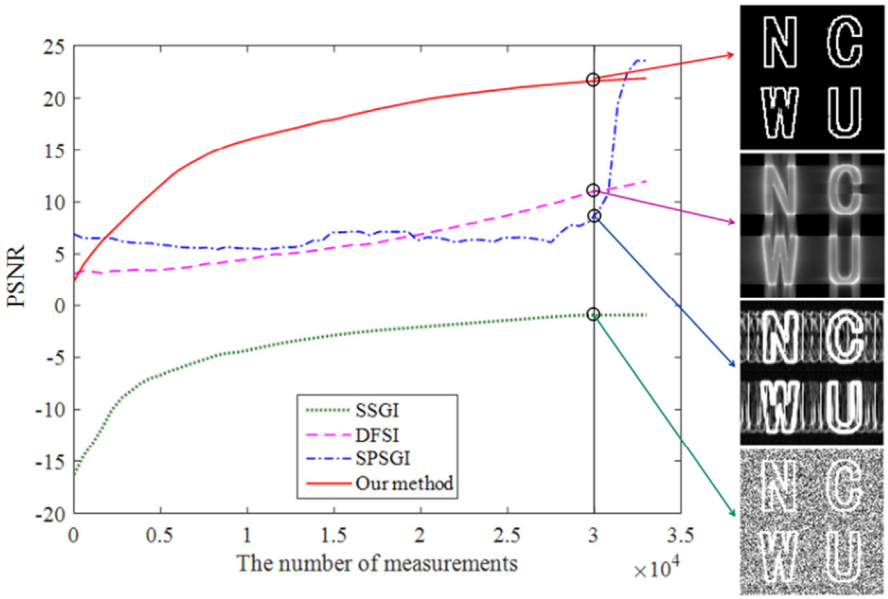


FIG. 8. The curves for PSNR varying with the number of measurements in SSGI, DFSI, SPSGI, and our proposed method, for the binary image.

and blurred for DFSI. Here we only take the binary image as an example and test the PSNRs of the imaging results, varying with the number of measurements, for SSGI, DFSI, SPSGI, and our method proposed in this paper. The curves are shown in Fig. 8. As can be seen from the results, our proposed method can realize high imaging quality when fewer measurements are adopted, although it cannot completely remove noise from the detected edge.

## V. CONCLUSION

In this paper we have proposed a novel SSGI technique to improve imaging speed and quality. Numerical simulations are carried out to verify its performance. However, owing to the imaging mechanism of SSGI, the results still contain serious noise. To solve the problem, we also explored a method to suppress the noise of SSGI results via CRL algorithms. In this method, two frame-edge-detection results are first generated by SSGI with the Sobel operator, and then a preprocessing step with a threshold and the CRL algorithm are applied in turn to reduce the noise. Compared to SPSGI and DFSI techniques, this method cannot completely remove noise from the detected edge, but it can realize high imaging quality with fewer measurements. Numerical simulations are carried out to verify the method's feasibility and effectiveness. Actually, the method proposed in this paper is simple, and so will take little operation time. The disadvantage of this method is that the CRL is invalid for noise adhering to the edge; some other effective algorithms still need to be further investigated.

## ACKNOWLEDGMENT

This work is supported by the National Natural Science Foundation of China (Grant No. 61475104, 61601183, and 61205003), Innovation Scientists and Technicians Troop Construction Projects of Henan Province (Grant No. CXTD 2014037), Project Plan of Key Scientific Research in University of Henan Province (Grant No. 19A510003), and Science and Technology Development Program in Henan Province (Grant No. 172102210368 and 182102310731).

## APPENDIX

Here, we give a further explanation for the edge-extraction process as follows. According to Eq. (1), Eq. (3) can be rewritten as

$$B_r^H=\sum_x\sum_y\begin{bmatrix}I_r(x+1,y-1)+2I_r(x+1,y)\\+I_r(x+1,y+1)-I_r(x-1,y-1)\\-2I_r(x-1,y)-I_r(x-1,y+1)\end{bmatrix}O(x,y) \tag{A1}$$

The average of all of the single-pixel detected data can be expressed as

$$\langle B^H\rangle=\frac{1}{M}\sum_{r=1}^{M}\left\{\sum_x\sum_y\begin{bmatrix}I_r(x+1,y-1)+2I_r(x+1,y)\\+I_r(x+1,y+1)-I_r(x-1,y-1)\\-2I_r(x-1,y)-I_r(x-1,y+1)\end{bmatrix}O(x,y)\right\} \tag{A2}$$

Thus, the formula for the horizontal edge, *i.e.* Eq. (5), can be further deduced by

$$\begin{aligned}
E_H(x,y)&=\frac{1}{M}\sum_{r=1}^{M}(B_r^H-\langle B^H\rangle)I_r(x,y)\\
&=\frac{1}{M}\sum_{r=1}^{M}\left\{\sum_x\sum_y\begin{bmatrix}I_r(x+1,y-1)+2I_r(x+1,y)\\+I_r(x+1,y+1)-I_r(x-1,y-1)\\-2I_r(x-1,y)-I_r(x-1,y+1)\end{bmatrix}O(x,y)\right\}\\
&\quad-\frac{1}{M}\sum_{r=1}^{M}\left\{\sum_x\sum_y\begin{bmatrix}I_r(x+1,y-1)+2I_r(x+1,y)\\+I_r(x+1,y+1)-I_r(x-1,y-1)\\-2I_r(x-1,y)-I_r(x-1,y+1)\end{bmatrix}O(x,y)\right\}I_r(x,y)\\
&=\frac{1}{M}\sum_{r=1}^{M}\left\{\begin{matrix}\sum_x\sum_y I_r(x+1,y-1)O(x,y)\\-\frac{1}{M}\sum_{r=1}^{M}\left[\sum_x\sum_y I_r(x+1,y-1)O(x,y)\right]\end{matrix}\right\}I_r(x,y)\\
&\quad+\frac{2}{M}\sum_{r=1}^{M}\left\{\begin{matrix}\sum_x\sum_y I_r(x+1,y)O(x,y)\\-\frac{1}{M}\sum_{r=1}^{M}\left[\sum_x\sum_y I_r(x+1,y)O(x,y)\right]\end{matrix}\right\}I_r(x,y)\\
&\quad+\frac{1}{M}\sum_{r=1}^{M}\left\{\begin{matrix}\sum_x\sum_y I_r(x+1,y+1)O(x,y)\\-\frac{1}{M}\sum_{r=1}^{M}\left[\sum_x\sum_y I_r(x+1,y+1)O(x,y)\right]\end{matrix}\right\}I_r(x,y)\\
&\quad-\frac{1}{M}\sum_{r=1}^{M}\left\{\begin{matrix}\sum_x\sum_y I_r(x-1,y-1)O(x,y)\\-\frac{1}{M}\sum_{r=1}^{M}\left[\sum_x\sum_y I_r(x-1,y-1)O(x,y)\right]\end{matrix}\right\}I_r(x,y)\\
&\quad-\frac{2}{M}\sum_{r=1}^{M}\left\{\begin{matrix}\sum_x\sum_y I_r(x-1,y)O(x,y)\\-\frac{1}{M}\sum_{r=1}^{M}\left[\sum_x\sum_y I_r(x-1,y)O(x,y)\right]\end{matrix}\right\}I_r(x,y)\\
&\quad-\frac{1}{M}\sum_{r=1}^{M}\left\{\begin{matrix}\sum_x\sum_y I_r(x-1,y+1)O(x,y)\\-\frac{1}{M}\sum_{r=1}^{M}\left[\sum_x\sum_y I_r(x-1,y+1)O(x,y)\right]\end{matrix}\right\}I_r(x,y)\\
&=\widetilde{O}(x+1,y-1)+2\widetilde{O}(x+1,y)+\widetilde{O}(x+1,y+1)\\
&\quad-\widetilde{O}(x-1,y-1)-2\widetilde{O}(x-1,y)-\widetilde{O}(x-1,y+1)\\
&=\nabla\widetilde{O}_H^{Sobel}(x,y)
\end{aligned} \tag{A3}$$

where $\widetilde{O}$ denotes the image retrieved by CGI, and $\nabla\widetilde{O}_H^{Sobel}(x,y)$ is the horizontal edge extracted by the Sobel operator. Therefore, the gradient operation for the illumination intensity patterns (Eq. (1)) is essentially equivalent to that for the captured images, so the horizontal edge of the object will be extracted from the horizontal intensity patterns $\{I_r^H(x,y)\}$.

The vertical edge of the object can be extracted by the same principle, and is expressed as

$$\begin{aligned} &= \widetilde{O}(x-1,y+1)+2\widetilde{O}(x,y+1)+\widetilde{O}(x+1,y+1) \\ &\quad -\widetilde{O}(x-1,y-1)-2\widetilde{O}(x,y-1)-\widetilde{O}(x+1,y-1) \\ &= \bigtriangledown \widetilde{O}_V^{Sobel}(x,y) \end{aligned} \tag{A4}$$

where $\bigtriangledown \widetilde{O}_V^{Sobel}(x,y)$ is the vertical edge extracted by the Sobel operator. From Eq. (A4), we know that the vertical edge of the object can also be extracted from the vertical intensity patterns $\{I_r^V(x,y)\}$.

The edge of the object will be obtained from

$$E(x,y) = \sqrt{[E_H(x,y)]^2 + [E_V(x,y)]^2} \tag{A5}$$

## REFERENCES


1. T. B. Pittman, Y. H. Shih, D. V. Strekalov, and A. V. Sergienko, "Optical imaging by means of two-photon quantum entanglement," Phys. Rev. A **52**, R3429-R3432 (1995).
2. R. S. Bennink, S. J. Bentley, and R. W. Boyd, ""Two-photon" coincidence imaging with a classical source," Phys. Rev. Lett. **89**, 113601 (2002).
3. A. Valencia, G. Scarcelli, M. D. Angelo, and Y. Shih, "Two-photon imaging with thermal light," Phys. Rev. Lett. **94**, 063601 (2005).
4. X. F. Liu, X. H. Chen, X. R. Yao, W. K. Yu, G. J. Zhai, and L. A. Wu, "Lensless ghost imaging with sunlight," Opt. Lett. **39**, 2314-2317 (2014).
5. Z. Zhang, X. Ma, and J. Zhong, "Single-pixel imaging by means of Fourier spectrum acquisition," Nat. Commun. **6**, 6225-6230 (2015).
6. L. Wang and S. M. Zhao, "Fast reconstructed and high-quality ghost imaging with fast Walsh-Hadamard transform," Photonics Res. **4**, 240-244 (2016).
7. W. Jue, Y. Renlong, X. Yu, S. Yanming, C. Yanru, and Z. Qi, "Ghost imaging with different speckle sizes of thermal light," J. Opt. Soc. Korea **20**, 8-12 (2016).
8. J. H. Shapiro, "Computational ghost imaging," Phys. Rev. A **78**, 061802 (2008).
9. Y. Bromberg, O. Katz, and Y. Silberberg, "Ghost imaging with a single detector," Phys. Rev. A **79**, 053840 (2009).
10. O. Katz, Y. Bromberg, and Y. Silberberg, "Compressive ghost imaging," Appl. Phys. Lett. **95**, 131110 (2009).
11. F. Ferri, D. Magatti, L. A. Lugiato, and A. Gatti, "Differential ghost imaging," Phys. Rev. Lett. **104**, 253603 (2010).
12. B. Sun, S. S. Welsh, M. P. Edgar, J. H. Shapiro, and M. J. Padgett, "Normalized ghost imaging," Opt. Express **20**, 16892-16901 (2012).
13. W. Wang, Y. P. Wang, J. Li, X. Yang, and Y. Wu, "Iterative ghost imaging," Opt. Lett. **39**, 5150-5153 (2014).
14. W. Wang, X. Hu, J. Liu, S. Zhang, J. Suo, and G. Situ, "Gerchberg-Saxton-like ghost imaging," Opt. Express **23**, 28416-28422 (2015).
15. X. F. Liu, X. R. Yao, R. M. Lan, C. Wang, and G. J. Zhai, "Edge detection based on gradient ghost imaging," Opt. Express **23**, 33802-33811 (2015).
16. T. Mao, Q. Chen, W. He, Y. Zou, H. Dai, and G. Gu, "Speckle-Shifting ghost imaging," IEEE Photonics J. **8**, 1-10 (2016).
17. L. Wang, L. Zou, and S. Zhao, "Edge detection based on subpixel-speckle-shifting ghost imaging," Opt. Commun. **407**, 181-185 (2018).
18. H. Ren, S. Zhao, and J. Gruska, "Edge detection based on single-pixel imaging," Opt. Express **26**, 5501-5511 (2018).
19. F. Jiang, S. Zhang, S. Wu, Y. Gao, and D. Zhao, "Multi-layered gesture recognition with kinect," J. Mach. Learn. Res. **16**, 227-254 (2015).
20. X. Chen, Y. Wang, Y. Wang, M. Ma, and C. Zeng, "Quantized phase coding and connected region labeling for absolute phase retrieval," Opt. Express **24**, 28613-28624 (2016).
21. M. B. Dillencourt, H. Samet, and M. Tamminen, "A general approach to connected-component labeling for arbitrary image representations," J. ACM **39**, 253-280 (1992).